SCIENTIFIC PAPERS
OF THE UNIVERSITY OF PARDUBICE
Series B
The Jan Perner Transport Faculty
15 (2009)

STABILITY OF HINGED SPHERICAL CAP SUBJECTED TO EXTERNAL PRESSURE

Petr PAŠČENKO, Pavel ŠVANDA

Department of Mechanics, Materials and Machine Parts

1.Introduction

The aim of this article is to perform a detail numerical analysis of the spherical cap subjected to an external pressure. The main task is to perform fully non-linear computational analyses in which both the material and geometrical nonlinearities are taken into consideration. The material nonlinearity enables a study of the limit state of plasticity while the geometrical nonlinearity displays the possible loss of stability. The problem is reduced to the spherical caps with hinged boundary conditions.

2.Theoretical background

The loss of stability is one of the limit states which may occur in an excessively loaded thin-wall structure. It flows from the shell theory that they can collapse in various ways depending on geometrical parameters, boundary conditions, loading conditions, material characteristics and initial imperfections. The stability collapse is induced by minimum load corresponding to a particular form of deformation. The membrane energy is converted to both the membrane and bending energy. As the membrane stiffness of the shell structures is several orders higher than the bending stiffness, the loss of stability is attended by large displacements of a wave character often visible to the naked eye.

Way of loss of stability

Bushnell D. describes in the introductory chapter of his book Computerized Buckling Analysis of Shells [1] basic types of loss of stability:

- Linear buckling
- Nonlinear axially symmetrical collapse
- Nonlinear buckling

Linear buckling (point B_L in Fig. 1) is characterized by a deformation of the structure in a new shape entirely different from the pre-buckling shape. The structure collapses when the curve tangent behind the bifurcation point is negative. The critical load corresponding to the bifurcation point is computed by means of the generalized eigenvalue theory.

Nonlinear axially symmetrical collapse (point A in Fig. 1) is characterized by decreasing stiffness of the structure with increasing load. In most cases, when the peak of the equilibrium curve is reached, the sudden loss of stability follows. The cap snaps through into its inverse position. The snap-through occurs in an axially symmetrical form along the curve 0AC.

Nonlinear buckling is characterized either by axially nonsymmetrical snap-through along the curve $0B_{N1}D$ or by nonlinear axially symmetrical collapse subsequently followed by axially nonsymmetrical snap-through along the curve $0AB_{N2}E$.

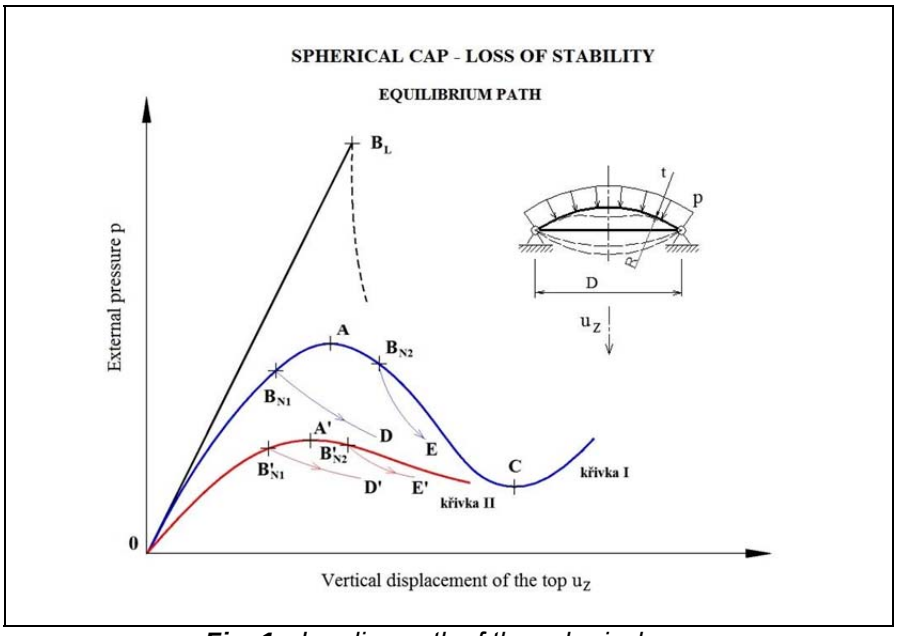

Fig. 1 *Loading path of the spherical cap*

The real structures with initial imperfections exhibit similar behavior, however, the loading curve (curve II*)* is lower than the loading curve valid for the *ideal structures*

(curve I). The collapse occurs again due to either the nonlinear buckling or nonlinear axially symmetrical collapse or nonlinear axially symmetrical collapse followed by nonlinear buckling.

Initial imperfection influence on loss of stability

The current technical standards and recommendations concerning stability of thin-walled shell structures [2], [3], [4], [5] provide needed analytical formulas convenient for the buckling analysis. The methods are based on the linear theory [6]. The equation (1) represents the linear partial differential equation of the spherical shell. The resulting external critical pressure is expressed in equation (2). The influence of both the material nonlinearity and initial imperfections are additionally taken into consideration.

$$\frac{D_t}{t}\nabla^6 w + \sigma\nabla^4 w + \frac{E}{R^2}\nabla^2 w = 0 \tag{1}$$

$$p_{KR} = 1{,}21 \cdot E \cdot \left(\frac{t}{R}\right)^2 \quad . \tag{2}$$

Primarily, the standard stability solution based on the *generalized eigenvalue problem* is performed. It results in the critical load of the ideal shell. However, this value is too optimistic in relation to a real imperfect structure. Therefore, some corrections regarding to initial imperfections are necessary. The initial imperfections are represented by variations in shape, real boundary conditions, real load and residual stresses. The standards provide various procedures to adjust results of the ideal shell to the real one.

It can be shown that the *imperfection sensitivity* of axially compressed cylindrical shells is the same as in the case of imperfection sensitivity of spherical shells loaded with an external pressure. Based on this fact, the following procedure for verification of spherical shell stability in elastic area may be adopted [3].

Stability of the axially compressed cylindrical shell:

$$\sigma_u = \frac{\alpha_0 \cdot \sigma_{KR}}{\gamma} \quad , \tag{3}$$

where the critical stress (buckling stress) is:

$$\sigma_{KR} = 0{,}605 \cdot E \cdot {}^{t}/_{R} \quad . \tag{4}$$

The ratio between the cylindrical and spherical shells can be expressed based on the *boiler formula* (5). It leads to the equation for the external critical pressure of the spherical shell:

$$p_{KR} = \frac{2 \cdot \sigma_{KR} \cdot t}{R} = \frac{2 \cdot \left(0{,}605 \cdot E \cdot \left({}^{t}/_{R}\right)\right) \cdot t}{R} = 1{,}21 \cdot E \cdot \left({}^{t}/_{R}\right)^2 \quad . \tag{5}$$

Finally, the stability of the real imperfect spherical shell in elastic era is:

$$p_u = \frac{\alpha_0 \cdot p_{KR}}{\gamma} \quad . \tag{6}$$

The reduction factor α_0 taking into account imperfections is determined using the expression:

$$\alpha_0 = \frac{0{,}83}{\sqrt{1+0{,}01 \cdot R/t}} \qquad \text{for R/t < 212}$$

$$\alpha_0 = \frac{0{,}70}{\sqrt{0{,}1+0{,}01 \cdot R/t}} \qquad \text{for R/t} \geq 212 \ . \tag{7}$$

The graphic interpretation of α_0 versus *R/t* is shown in Fig. 2

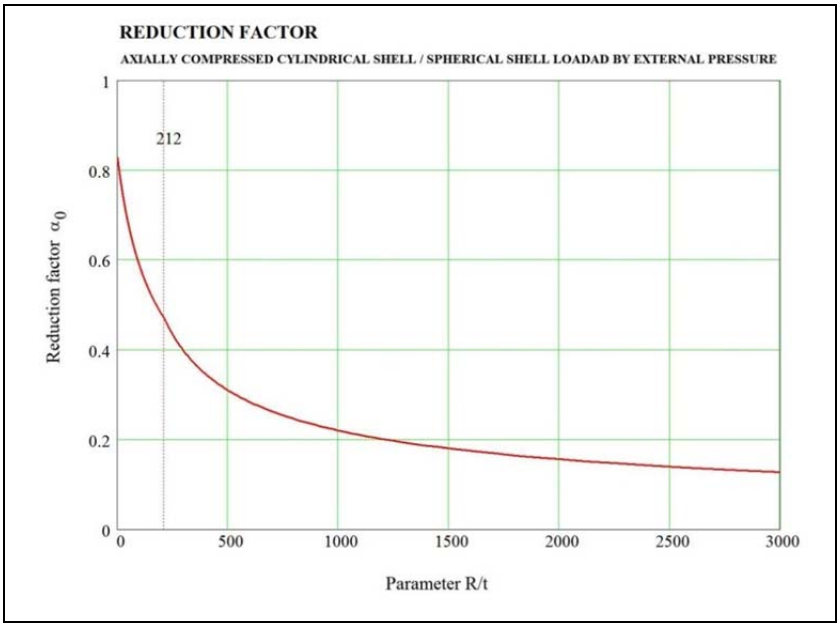

Fig. 2 *Reduction factor according to ECCS [3]*

Elastic-plastic material behavior

Now, the influence of plasticity is necessary to take into consideration. The rigid-plastic material behavior is implemented into the following mathematical formulas.

$$\sigma_u = \frac{\alpha_0 \cdot \sigma_{KR}}{\gamma} \qquad \text{for} \quad \alpha_0 \sigma_{KR} < \frac{1}{2} \cdot f_y \tag{8}$$

$$\sigma_u = f_y \cdot \left[1 - 0{,}4123 \cdot \left(\frac{f_y}{\alpha_0 \sigma_{KR}}\right)^{0{,}6}\right] \quad \text{for} \quad \alpha_0 \sigma_{KR} \geq \frac{1}{2} \cdot f_y \ . \tag{9}$$

Both the equations are graphically described in Fig. 3. The safety factor for short thick shells is $\gamma = 4/3 > 1$ since the plasticity there completely overcomes the stability. The transition from the design stress σ_u to the design pressure p_u is again performed by means of the boiler formula:

$$p_u = \frac{2 \cdot \sigma_u \cdot t}{R} \quad . \tag{10}$$

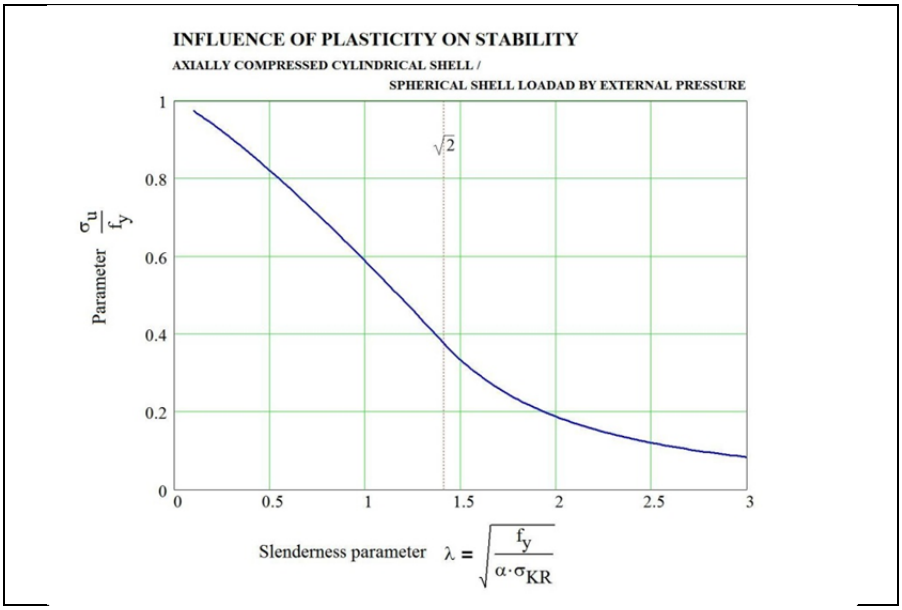

Fig. 3 *Influence of plasticity on stability*

3.Numerical stability analysis of hinged spherical cap

Ideal structure

The following text is devoted to a detail numerical analysis of an ideal shallow spherical cap with a hinged lower edge. The cap is loaded with an external pressure *p*. The finite element computational model (see Fig. 4) is assembled for this purpose. The model is assembled of 3076 elements SHELL4T. The cylindrical coordinate system *0xyz* with radial direction *x*, circumferential direction *y* and axis *z* identical with the axis of the cap is defined. The ideal structure without initial imperfections is considered. The basic dimensions of the analyzed cap are R=1200 mm, D=1400 mm. The thickness varies from 3 to 12 mm. The analysis is completed with two modifications of radius R=2400 mm and 3600 mm.

The stainless steel material 1.4301 [9] with Young's modulus E=2E+5 MPa and yield strength f_y=250 MPa at temperature T=20°C is prescribed. The material nonlinearity in the form of von Mises's bilinear model with modulus E_T=E/10000=20 MPa is adopted (elastic-plastic material, see Fig. 5).

The results of the computer analyses are performed in Tab. 1 ÷ Tab. 3. To better illustrate, the results are also presented in a graphical form (see Fig. 6 ÷ Fig. 8). The diagram represents the external pressure *p* dependence on parameter *R/t*.

The diagram consists of three curves:

- LBA – linear buckling analysis,
- NEA – nonlinear elastic analysis,
- NPA – nonlinear elastic-plastic analysis.

***Tab. 1** Results: R=1200 mm, D=1400 mm, R/D=0.857, hinged*

t	12	10	8	6	5	4	3.333	3
R/t	100	120	150	200	240	300	360	400
p_{LP}	4.595	3.771	2.932	2.083	1.672	1.261	0.993	0.855
p_{LE}	16.220	11.130	7.177	4.146	2.875	1.863	1.311	1.068
ξ_L	3.530	2.951	2.448	1.990	1.719	1.477	1.320	1.249
p_{KR}	24.463	17.106	10.954	6.177	4.294	2.766	1.926	1.566
p_{KRA}	24.200	16.806	10.756	6.050	4.201	2.689	1.867	1.513
ξ_{KR}	0.989	0.982	0.982	0.979	0.978	0.972	0.969	0.966

***Tab. 2** Results: R=2400 mm, D=1400 mm, R/D=1.714, hinged*

t	12	10	8	6.667	6	5.333	5	4	3.333	3
R/t	200	240	300	360	400	450	480	600	720	800
p_{LP}	2.049	1.648	1.246	0.979	0.846	0.721	0.659	0.454	0.329	0.270
p_{LE}	4.355	3.060	1.984	1.358	1.091	0.853	0.741	0.454	0.329	0.270
ξ_L	2.125	1.857	1.592	1.387	1.290	1.183	1.124	1.000	1.000	1.000
p_{KR}	6.163	4.241	2.736	1.890	1.542	1.213	1.066	0.684	0.476	0.387
p_{KRA}	6.050	4.201	2.689	1.867	1.513	1.195	1.050	0.672	0.467	0.378
ξ_{KR}	0.982	0.991	0.983	0.988	0.981	0.985	0.985	0.982	0.981	0.977

***Tab. 3** Results: R=3600 mm, D=1400 mm, R/D=2.571, hinged*

t	12	10	9	8	7.5	6	5	4.5	4	3
R/t	300	360	400	450	480	600	720	800	900	1200
p_{LP}	1.204	0.945	0.821	0.696	0.630	0.449	0.327	0.262	0.202	0.111
p_{LE}	1.904	1.270	1.017	0.804	0.713	0.467	0.329	0.262	0.202	0.111
ξ_L	1.581	1.344	1.239	1.155	1.132	1.040	1.006	1.000	1.000	1.000
p_{KR}	2.732	1.869	1.521	1.221	1.066	0.679	0.474	0.382	0.304	0.171
p_{KRA}	2.689	1.867	1.513	1.195	1.050	0.672	0.467	0.378	0.299	0.168
ξ_{KR}	0.984	0.999	0.995	0.979	0.985	0.990	0.985	0.990	0.984	0.982

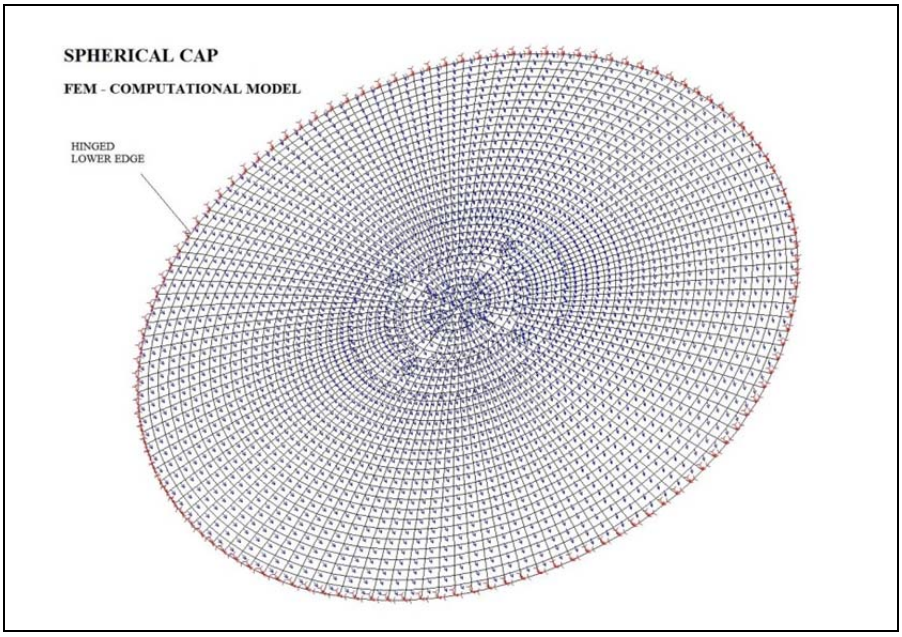

Fig. 4 *FEM computational model*

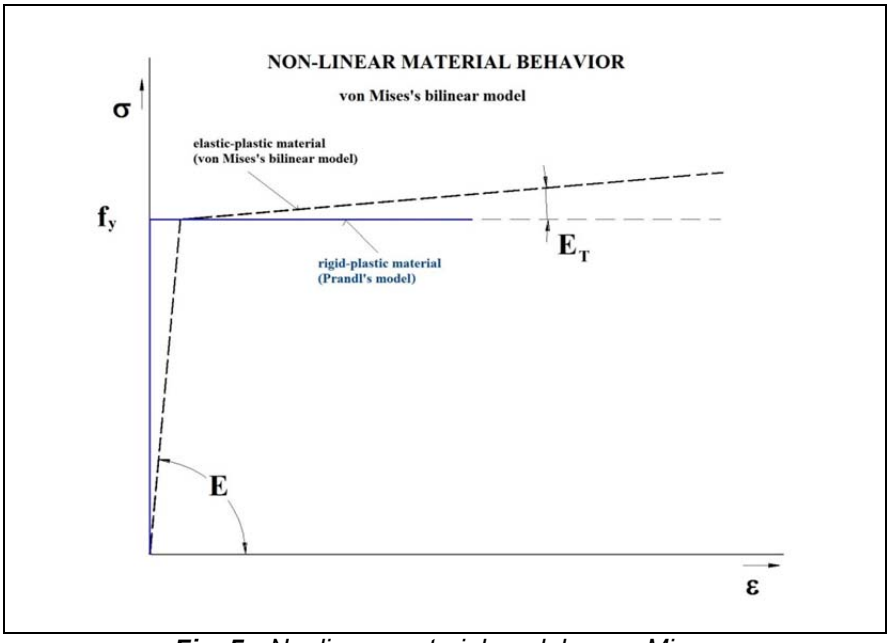

Fig. 5 *Nonlinear material model – von Mises*

Firstly, it is clear that the curves decrease with an increasing parameter *R/t*. The difference between the results *LBA* and *NPA* is not as big as could be expected in case

of the cap with free lower edge in the radial direction. The ratio p_{CR}/p_{LE} is located in a narrow interval *1.4÷1.55*. For that case, the following slightly conservative equation can be adopted:

$$p_{LE} = p_{KR}/1{,}6 \ . \tag{11}$$

Furthermore, it is worth noting that the critical pressures p_{CR} computed numerically for a spherical cap are practically identical with the critical pressures p_{CRA} received analytically for a full spherical shell (2). The slightly higher numerical results can be explained by the stiffer discrete numerical model in comparison with the real continuum. Then equation (11) can be rewritten in the form:

$$p_{LE} = p_{KRA}/1{,}6 \ . \tag{12}$$

However, the limit pressure p_{LE} may not be a real limit value of the ideal shell. In most cases, the nonlinear collapse can occur in an elastic-plastic area due to limit pressure p_{LP} which can be significantly lower than p_{LE}. The ratio $\xi_L = p_{LE}/p_{LP}$ versus parameter *R/t* is performed in Tab. 1÷3. The maximum value $\xi_L = 3.53$ corresponds to the cap with *R/t=100*, while minimum $\xi_L \approx 1.0$ to the cap with $R/t \geq 600$. It is clear that the caps with lower *R/t* are influenced by plastic deformations more than thin-walled caps.

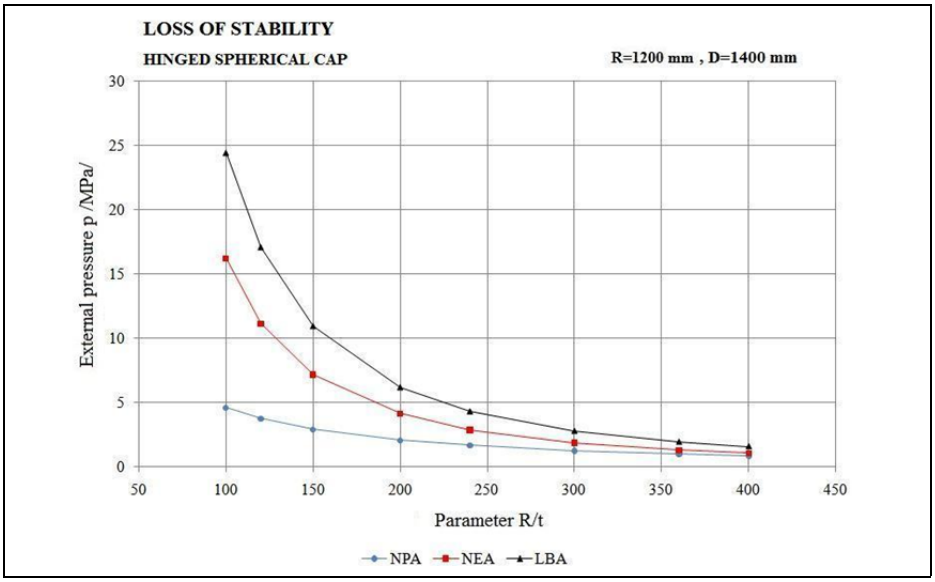

Fig. 6 *Pressure p_{CR}, p_{LE}, p_{LP} versus parameter R/t, R=1200 mm*

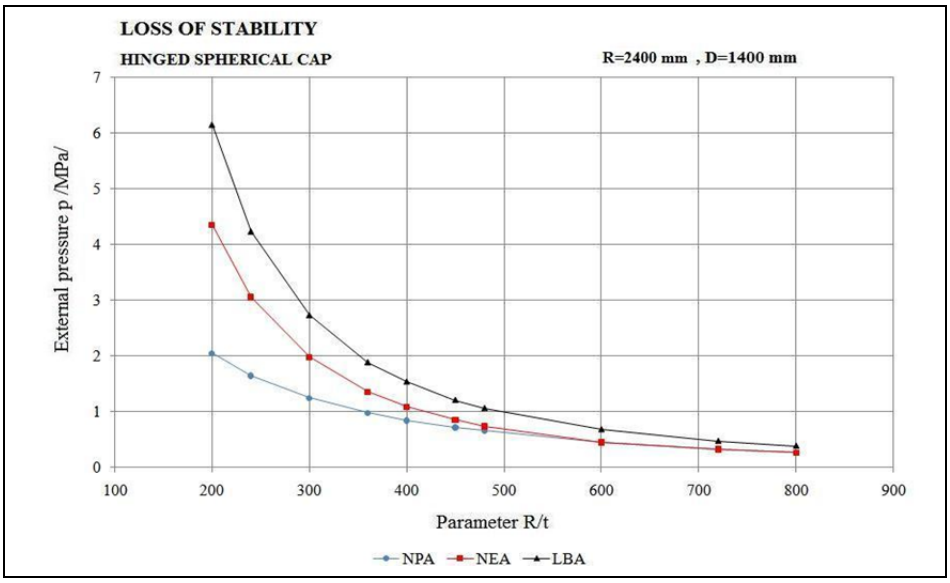

Fig. 7 *Pressure p_{CR}, p_{LE}, p_{LP} versus parameter R/t, R=2400 mm*

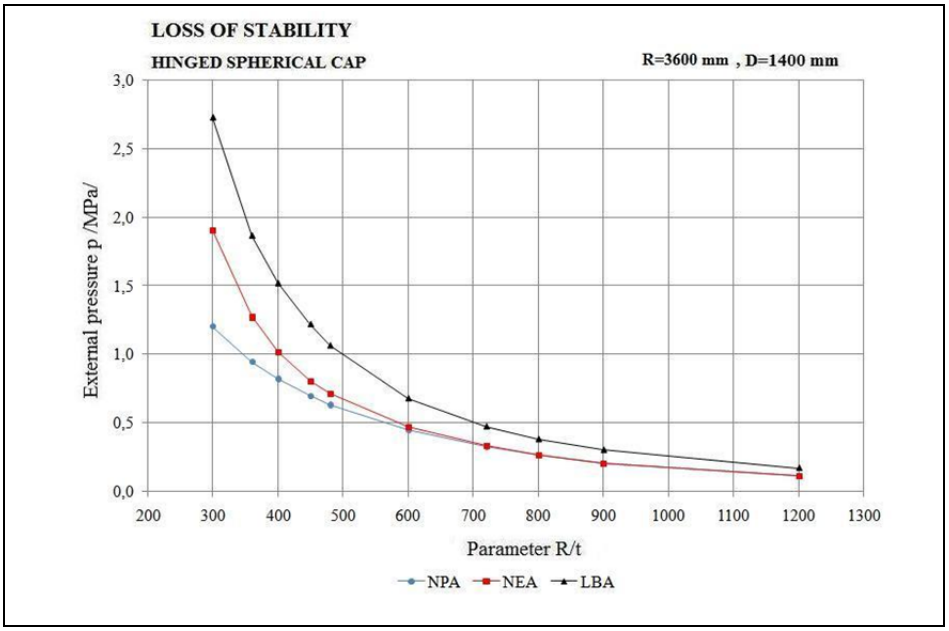

Fig. 8 *Pressure p_{CR}, p_{LE}, p_{LP} versus parameter R/t, R=3600 mm*

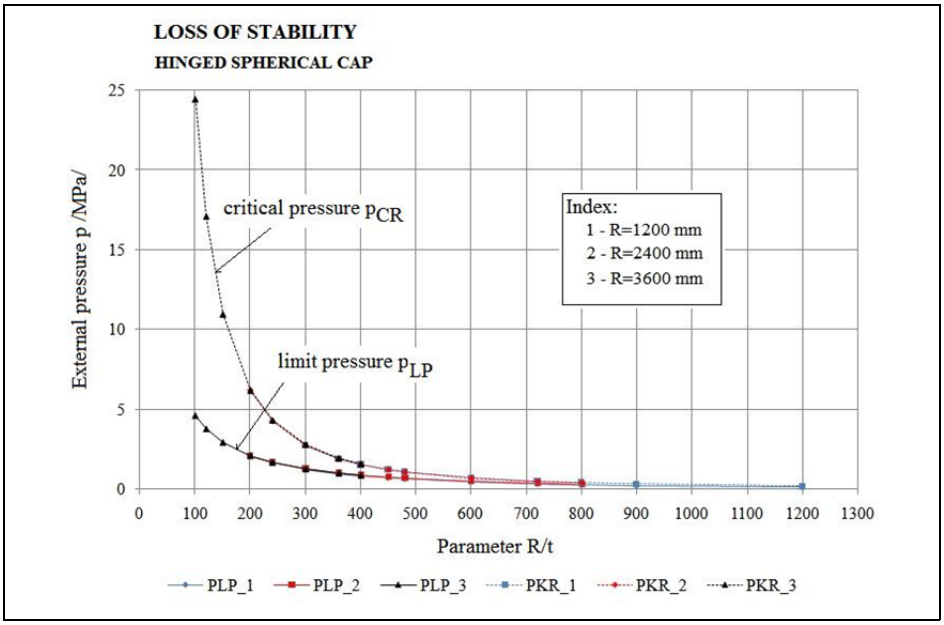

Fig. 9 *Pressure p_{CR}, p_{LP} versus parameter R/t*

The study of the curves in Fig. 6 ÷ Fig. 8 shows that they may be expressed in a form of a regression curve

$$p_L = K \cdot E \cdot \left(\frac{t}{R}\right)^m \quad . \tag{13}$$

The regression coefficients are performed in Tab. 4. This regression formula is now suitable for a practical use. To better illustrate the situation, the ratio p_{CR}-*R/t* and p_{LP}-*R/t* is shown in Fig. 9.

Tab. 4 *Regression coefficients, hinged lower edge*

GEOMETRY	R/D=0.857		R/D=1.714		R/D=2.571	
KOEFFICIENTS	K	m	K	m	K	m
p_{LP}	6.248E-3	1.211	2.475E-2	1.456	0.1105	1.723
p_{LE}	0.6538	1.956	1.0503	2.032	0.9134	2.016
p_{KR}	1.1432	1.985	1.1953	1.995	1.1882	1.995
R/t	100÷400		200÷800		300÷1200	

Real structure

Now, it is necessary to open the question concerning the initial imperfections. The limit pressure p_{LP} is not a limit pressure of the real cap since the initial imperfections can significantly reduce this value. The initial imperfections are considered through the reduction factor α_0 (7). Several possible ways to determine a design pressure of the real spherical cap p_u are shown in the following text:

- based on the critical pressure p_{CRA} of the ideal spherical shell,
- based on the limit pressure p_{PL} of the ideal spherical cap,

- based on the full nonlinear numerical analysis of the real imperfect spherical cap.

The *first way* leads to the design pressure computed analytically through the equations (5)÷(10). The *second way* is based on the nonlinear limit pressure p_{PL} computed numerically and adjusted directly to the real structure by means of the reduction factor α_0

$$p_u = \frac{\alpha_0 p_{LP}}{\gamma} \quad . \tag{14}$$

The following table (tab. 5.) performs the design pressure p_{u1} (way 1) and p_{u2} (way 2). As he results are considerably different the further research in this area is needed.

The last way (way 3) is somewhat complicated and its deeper analysis is a question of the further research. The supposed ratio α_0 versus parameter *R/t* for various boundary conditions is shown in Fig. 10. The increasing reduction factor α_0 with stiffer boundary conditions can be expected.

***Tab. 5** Limit pressure of the ideal and real hinged shallow cap*

R/t	100	120	150	200	240	300	360
p_{u1}	3.539	2.769	2.005	1.250	0.864	0.505	0.319
P_{u2}	2.023	1.583	1.155	0.737	0.547	0.359	0.258

continuation of table 5.

400	450	480	600	720	800	900	1200
0.245	0.183	0.156	0.089	0.057	0.044	0.033	0.016
0.213	0.170	0.149	0.095	0.064	0.048	0.035	0.017

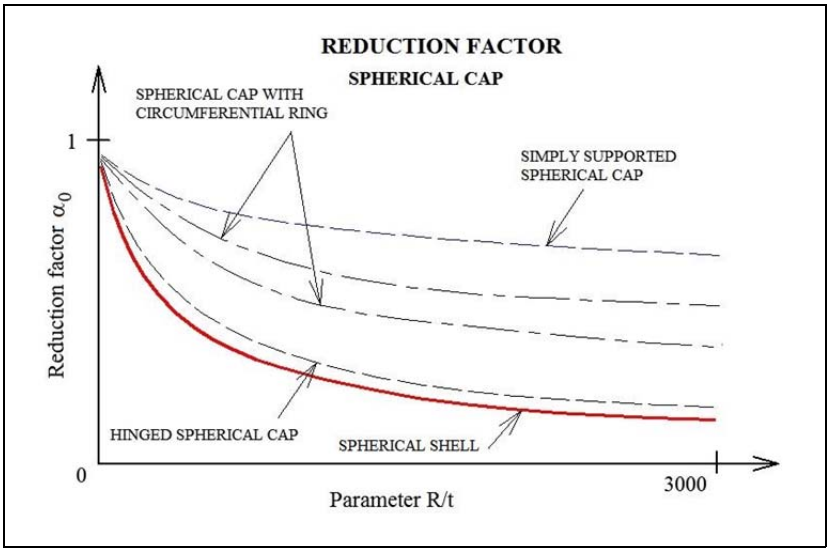

***Fig. 10** Reduction factor versus parameter R/t*

4.Example

The following text is devoted to the example concerning the numerical analysis of the spherical cap with radius R=3600 mm, diameter D=1400 mm and thickness t=8 mm. Von Mises's elastic-plastic bilinear model of material with real material characteristics E=2E+5 MPa, μ=0.3, f_y=250 MPa and E_T=20 MPa is considered (stainless steel 1.4301 [5]). The nonlinear computational analysis is governed by Riks's arc-length control procedure. The axially-symmetrical initial imperfection with amplitude w_{z0}=6 mm is prescribed (cylindrical coordinate system *0xyz* is used).

The equilibrium path is shown in Fig. 11. It represents the loading pressure *p* dependence on vertical displacement u_z of the center of the cap. At the beginning the model performs a linear behavior. At pressure p≈0.33 MPa the stiffness begins to decrease. It is caused by non-linear nature of the structure. The plasticity of the boundary elements can contribute to this phenomenon. The non-linear axially-symmetrical collapse occurs at point A (step 24 of the non-linear computational procedure). The non-linear collapse of the cap into its inverse position is starting. The deformed shape at the point A is shown in Fig. 12. However, the axially symmetrical collapse is suddenly disturbed at point B by axially non-symmetrical non-linear buckling. The deformed shape in step 158 is shown in Fig. 13. The analysis is ended in step 419 where the cap is close to its inverse position - again almost axially symmetrical shape (see Fig. 14).

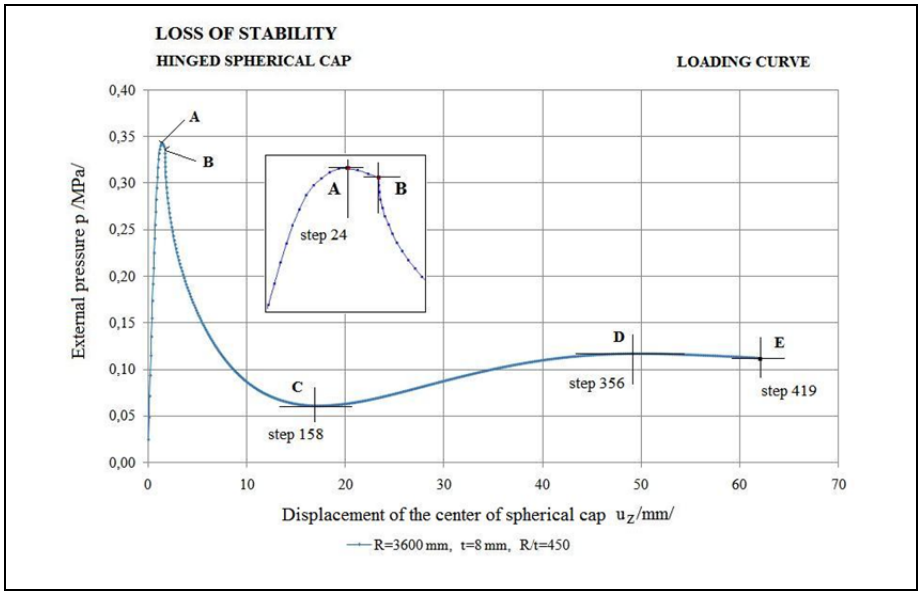

Fig. 11 *Loading curve (equilibrium curve)*

The resulting values important for a design are shown in Fig. 15, where

p_{CR}=1.221 MPa … critical pressure of ideal spherical cap,
p_{LE}=0.804 MPa … elastic limit pressure of ideal cap,
p_{LP}=0.696 MPa … elastic-plastic limit pressure of ideal cap,
p_{LEI}=0.425 MPa … elastic limit pressure of real imperfect cap,
p_{LPI}=0.343 MPa … elastic-plastic limit pressure of real imperfect cap.

It flows from the results that the defined initial imperfection significantly reduced the stability of the cap. In this case is the ratio $p_{LP}/p_{LPI}\approx 2.0$.

In most practical cases, the general imperfections prescribed by corresponding standards are considered instead of the real measured imperfections. The first two ways of tacking the stability problem are performed

- according to ECCS with standard reduction factor α_0

$$p_{u1} = \frac{\alpha_0 p_{LP}}{\gamma} = \frac{0{,}326 \cdot 0{,}696}{4/3} = 0{,}170\ MPa$$

- according to ECCS with supposed imperfection w_0=6 mm

$$p_{u2} = \frac{p_{LPI}}{\gamma} = \frac{0{,}343}{4/3} = 0{,}257\ MPa.$$

To decide which result is closer to the truth, the complex analysis of initial imperfections on the spherical cap is needed. That analysis is taken as a subject of future research.

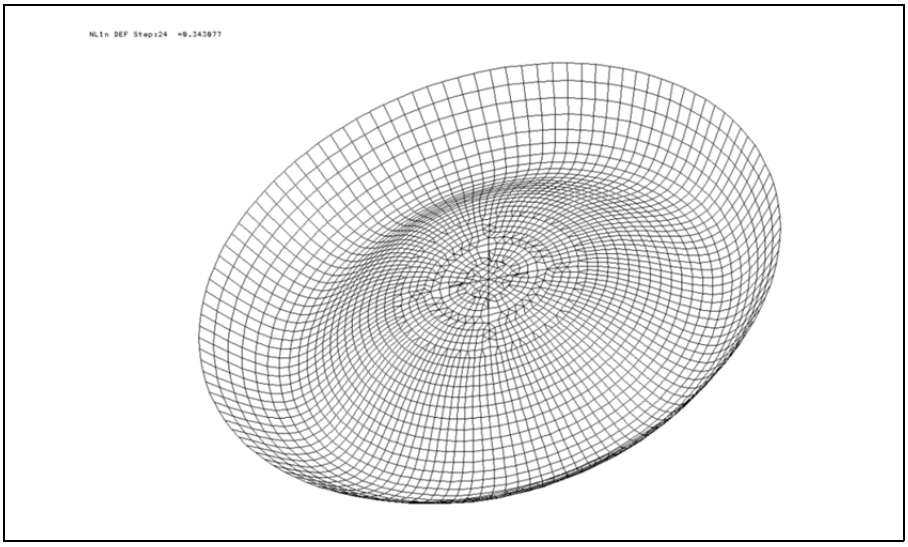

Fig. 12 *Deformed shape - step 24*

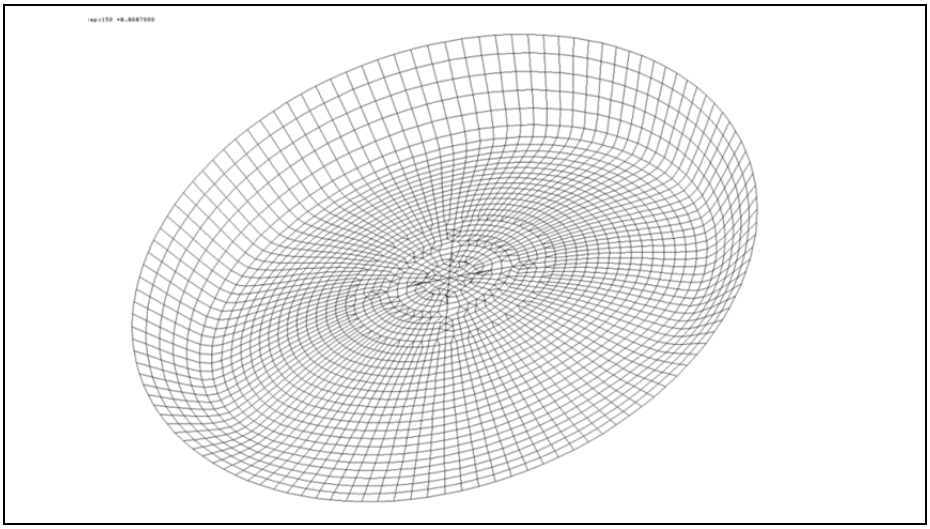

Fig. 13 *Deformed shape - step 158*

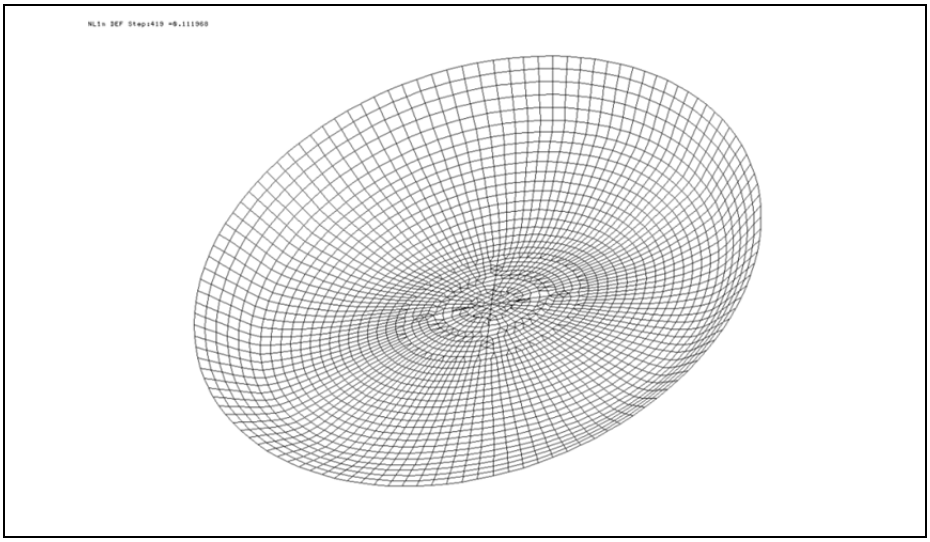

Fig. 14 *Deformed shape - step 419*

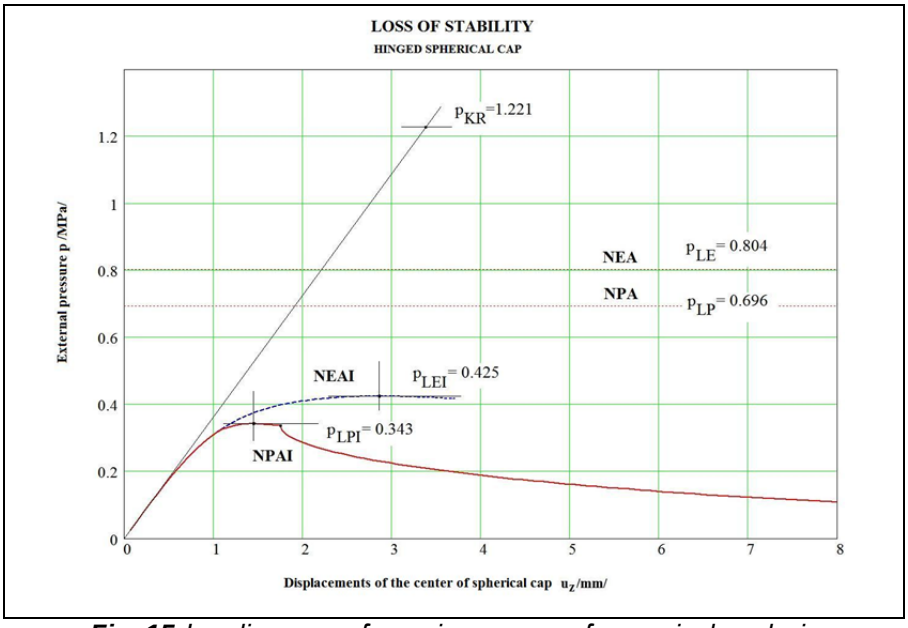

Fig. 15 *Loading curve for various cases of numerical analysis*

CONCLUSION

The article is aimed at stability of the spherical cap with the hinged lower edge. It is shown that the critical pressure of the cap is broadly in line with the critical pressure of the spherical cap. Further, the limit pressure in elastic area may by approximately expressed in form $p_{LE} \approx p_{CR}/1.6$. The influence o plasticity and initial imperfections on the stability of the real spherical cap can be finally computed, for example, on the basis of the European Recommendation [3]. The slightly conservative results are expected. The more precise influence of the initial imperfections on the stability of the spherical cap is a matter of further research.

Submited: 02.03.2010

References

1. Bushnell D. *Computerized buckling analysis of shells.* Martinus Nijhoff Publishers. Dordrecht. ISBN 90-247-3099-6 (1985).
2. DIN 18800, part.4. *Structural steelwork. Analysis of safety against buckling of shells. German norm*. Beuth Verlag GmbH, Berlin (1990).
3. ECCS-Buckling of Steel Shells. European Design Recommendations. Fourth edition, Published by ECCS (1988).
4. ECCS (2008) Buckling of Steel Shells. European Design Recommendations. Fifth edition, Published by ECCS, *ISBN* 92-9147-000-92.

5. EN 1993-1-6. *Design of steel structures – Part 1-6: Strength and Stability of Shell Structures*. European Committee for Standardization (2007).
6. Volmir A.C.*Ustojčivosť uprugich sistěm.* Gosudarstvennoe izdastělstvo fiziko-matematiceskoj literatury. Moskva (1963).
7. FEM Computer program *COSMOS/M, Version 2.95* by SRAC (Structural Research and Analysis Corporation), Los Angeles, California.
8. Zienkiewicz O.C. *The Finite Element Method in Engineering Science.* The second edition. McGRAW-HILL, London, 07 094138 6 (1971).
9. EN 10028-7. *Flat products made of steel for pressure purposes – Part 7: Stainless steels* (2000).

Resumé

STABILITA KLOUBOVĚ ULOŽENÉHO KULOVÉHO VRCHLÍKU ZATÍŽENÉHO VNĚJŠÍM TLAKEM

Petr PAŠČENKO, Pavel ŠVANDA

Tenkostěnný kulový vrchlík zatížený vnějším tlakem vykazuje obecně nelineární chování. U kloubově uloženého vrchlíku s neposuvným okrajem v radiálním směru není toto nelineární chování tak výrazné. Z lineární analýzy kritického zatížení plyne, že stabilitní únosnost kulového vrchlíku je prakticky shodná se stabilitní únosností kulové skořepiny. Z nelineární elastické analýzy dále vyplývá, že mezi kritickým tlakem a mezním tlakem platí přibližný vztah $p_{CR}/p_{LE}=1{,}6$. Na základě toho lze počítat mezní elastický vnější tlak ideálního vrchlíku p_{LE} pomocí základního vztahu pro kritický vnější tlak kulové skořepiny p_{CRA}, tzn. $p_{LE}\approx p_{CR}/1.6\approx p_{CRA}/1{,}6$. Přepočet na mezní tlak reálného vrchlíku v pružně-plastickém oboru lze provést pomocí redukčního faktoru α_0 a pomocí diagramu na obrázku 3. Hlubší analýza vlivu počátečních imperfekcí na stabilitní únosnost kulového vrchlíku je předmětem dalšího výzkumu.

Summary

STABILITY OF HINGED SPHERICAL CAP SUBJECTED TO EXTERNAL PRESSURE

Petr PAŠČENKO, Pavel ŠVANDA

The thin-walled spherical cap loaded by an external pressure generally performs a non-linear behavior. This phenomenon is not as significant in case of the hinged cap with restricted movements in the radial direction. The linear analysis of the critical load shows that stability of the cylindrical cap is practically identical to stability of the cylindrical shell. In addition, the non-linear analysis further leads to the conclusion that the ratio between critical pressure and limit pressure might be expressed by formula $p_{CR}/p_{LE}=1.6$. Based on these facts, the limit elastic pressure p_{LE} of an ideal cap can be derived from a critical external pressure p_{CRA} of the spherical shell $p_{LE}\approx p_{CR}/1.6\approx p_{CRA}/1.6$. Conversion of p_{LE} to the limit pressure of a real spherical cap in elastic-plastic area p_u might be performed by means of the procedure provided by ECCS [3]. The influence of initial imperfections on stability of the spherical cap is a subject of further research.

Zusammenfassung

DIE STABILITÄT DER VON AUSSENDRUCK AUSGESETZTE DREHBARE KALOTTE

Petr PAŠČENKO, Pavel ŠVANDA

Die dünnwandige Kalotte durch einen Aussendruck ausgesetzt führt im Allgemeinen einem nichtlinearen Verhalten. Dieses Phänomen ist nicht als erheblich im Fall einen aufklappbaren Deckel mit eingeschränkten Bewegungsmöglichkeiten in radialer Richtung. Die lineare Analyse der kritischen Belastung zeigt, dass die Stabilität der zylindrischen Kappe ist praktisch identisch mit der Stabilität der zylindrischen Schale. Darüber hinaus ist die nicht-lineare Analyse führt weiter zu dem Schluss, dass das Verhältnis zwischen kritischen Druck und Druck zu begrenzen Formel ausgedrückt werden könnten $p_{CR}/p_{LE}=1.6$. Auf der Grundlage der Fakten ist die Obergrenze elastischen Druck p_{LE} einer idealen Kappe von einem kritischen Druck p_{CRA} der Kugelschale abgeleitet werden $p_{LE}\approx p_{CR}/1.6\approx p_{CRA}/1.6$. Umwandlung von p_{LE}" bis an die Grenze Druck einer realen Kalotte in elastisch-plastischen Bereich p_U könnte durch das Verfahren, nach ECCS vorgesehen durchgeführt werden [3]. Der Einfluss der ersten Unvollkommenheiten auf die Stabilität der Kalotte ist Gegenstand weiterer Forschung.